Published in final edited form as:
Cancer Prev Res (Phila). 2013 November ; 6(11): . doi:10.1158/1940-6207.CAPR-13-0227.

The Parity-Associated Microenvironmental Niche in the Omental Fat Band is Refractory to Ovarian Cancer Metastasis

Courtney A. Cohen[1], **Amanda A. Shea**[2], **C. Lynn Heffron**[1], **Eva M. Schmelz**[2,*], and **Paul C. Roberts**[1,*]

[1]Department of Biomedical Sciences and Pathobiology, Virginia Polytechnic Institute and State University, Blacksburg, VA, United States

[2]Department of Human Nutrition, Foods and Exercise, Virginia Polytechnic Institute and State University, Blacksburg, VA, United States

Abstract

Ovarian cancer is an insidious and aggressive disease of older women, typically undiscovered prior to peritoneal metastasis due to its asymptomatic nature and lack of early detection tools. Epidemiological studies suggest that child-bearing (parity) is associated with decreased ovarian cancer risk, although the molecular mechanisms responsible for this phenomenon have not been delineated. Ovarian cancer preferentially metastasizes to the omental fat band (OFB), a secondary lymphoid organ that aids in filtration of the peritoneal serous fluid (PSF) and helps combat peritoneal infections. In the present study we assessed how parity and age impact the immune compositional profile in the OFB of mice, both in the homeostatic state and as a consequence of peritoneal implantation of ovarian cancer. Using fluorescence-activated cell sorting analysis and quantitative realtime PCR, we found that parity was associated with a significant reduction in omental monocytic subsets and B1-B lymphocytes, correlating with reduced homeostatic expression levels of key chemoattractants and polarization factors (*Ccl1*, *Ccl2*, *Arg1*, *Cxcl13*). Of note, parous animals exhibited significantly reduced tumor burden following intraperitoneal implantation compared to nulliparous animals. This was associated with a reduction in tumor-associated neutrophils and macrophages, as well as in the expression levels of their chemoattractants (*Cxcl1*, *Cxcl5*) in the OFB and PSF. These findings define a pre-existing "parity-associated microenvironmental niche" in the OFB that is refractory to metastatic tumor seeding and outgrowth. Future studies designed to manipulate this niche may provide a novel means to mitigate peritoneal dissemination of ovarian cancer.

Keywords

Ovarian Cancer; Parity; Leukocytes; Omental fat band

INTRODUCTION

Ovarian cancer is responsible for 140,000 deaths a year in women worldwide (1) with one of the highest incidence-to-death ratios in the US due to late detection, tumor heterogeneity and

*Corresponding authors. Dr. Paul C. Roberts, Department of Biomedical Sciences and Pathobiology, Virginia Tech, Integrated Life Sciences Building, 1981 Kraft Drive [0913], Blacksburg, Va. 24061, Tel: 540-231-7948, pcroberts@vt.edu And Dr. Eva M. Schmelz, Department of Human Nutrition, Foods and Exercise, Virginia Tech, Integrated Life Sciences Building, 1981 Kraft Drive [0913], Blacksburg, Va. 24061, Tel: 540-231-7948, eschmelz@vt.edu.

Disclosure:
The authors declare no conflict of interest.

a high rate of metastasis (2). However, epidemiological studies indicate that among other factors, parity (child-bearing) may provide protection against the development of ovarian cancer (3). Nonetheless, little is known about the persistent molecular and cellular changes that modulate ovarian cancer development as a result of child-bearing.

As a largely asymptomatic disease in the early stages, ovarian cancer is rarely detected prior to metastasis. During metastasis ovarian cancer cells exfoliate from the primary tumor, disseminate throughout the peritoneal cavity in the serous fluid and preferentially seed in the omental fat band (OFB) (4). As the primary metastatic site, it is typically removed during surgical tumor debulking to slow disease progression. The OFB is considered a secondary lymphoid organ, contributing to immunosurveillance in the peritoneal cavity and its removal results in impaired anti-bacterial responses in the abdomen and increased risk of subsequent infections (5). It is composed of fatty tissue interspersed with immune cell aggregates or “milky spots”(6), consisting of leukocytes, stem and progenitor cells, fibroblasts and endothelial cells (7) collectively referred to as the stromal vascular fraction (SVF). Disseminated tumor cells adhere to milky spots within hours (8), promoting a pro-tumorigenic microenvironment that supports subsequent tumor outgrowth (6,8,9). However, the complex and dynamic interactions between metastatic cancer cells and leukocytes within the OFB have not been well characterized.

We have shown previously that the homeostatic immune microenvironment of the OFB significantly differs from that of other intraperitoneal fat depots with a distinct leukocyte profile, and a robust cytokine signaling network (10). It is unknown how this immune microenvironment is impacted by aging or parity, which may have critical implications for the generation of a metastatic niche that determines successful tumor adherence and outgrowth. However, epidemiological studies have reported increased ovarian cancer incidence in older women but a protective effect associated with parity (11). Here, we postulated that parity may induce changes in the OFB that result in a pre-existing immune microenvironment that is protective against cancer metastasis. As child-bearing is inherently associated with an older demographic, we chose three sets of female mice to distinguish between age- and parity-specific changes: five-month old nulliparous young adults, eleven-month old nulliparous mature adults, and twelve-month old mature parous adults. Given its importance as a primary metastatic site, in the present study we comparatively characterized the SVF and gene expression profiles of the OFB as a function of age and parity.

MATERIALS AND METHODS

Cell lines

The mouse ovarian surface epithelial (MOSE) cell model utilized in this study was developed from C57BL/6 mice and characterized previously (12). Tumorigenic MOSE cells were passaged once in vivo by intraperitoneal (i.p.) injection into C57BL/6 mice and re-collected via peritoneal lavage following a 4–6 week incubation period to select for a more aggressive phenotype. These MOSE cell variants (MOSE-L_{FFLv}) were subsequently transduced with firefly luciferase (FFL) lentiviral particles (GeneCopoeia) as described (13) to facilitate live *in vivo* imaging of cancer cell outgrowth. The characteristics of MOSE-L_{FFLv} will be reported elsewhere. MOSE-L_{FFLv} cells were routinely maintained in high glucose DMEM (Invitrogen), supplemented with 4% fetal bovine serum (Hyclone), 100mg/ml penicillin and streptomycin and 4μg/ml puromycin (lentiviral particles utilize a puromycin resistance marker for selection of transduced cells).

Animals

Female C57BL/6 mice (Harlan Laboratories) were housed five per cage in a controlled environment (12 hour light/dark cycle at 21°C) with free access to water and food (18% protein rodent chow, Teklad Diets). Young adult nulliparous mice (5 months of age, 21g average body weight), mature adult nulliparous mice (11 months of age, 30g average body weight) and mature parous mice (12 months of age, 31g average body weight) were sacrificed by CO_2 asphyxiation. Mouse studies were conducted in accordance with the guidelines approved by the Virginia Tech Institutional Animal Care and Usage Committee.

MOSE-L_{FFLv} injection

Young adult nulliparous and mature parous mice (n=10 per group) were injected i.p. with either 1×10^4 MOSE-L_{FFLv} cells in 300uL sterile calcium- and magnesium-deficient phosphate buffered saline ($PBS^{-/-}$), or mock-injected ($PBS^{-/-}$ alone) and sacrificed at 21 days post-injection.

Peritoneal cancer index (PCI)

In order to quantify relative tumor burden at the time of sacrifice, the PCI was determined as described previously (14,15), with minor modifications. The original PCI was adapted to apply to tumor size and region in mice; “quadrant areas” were modified to represent distinct organs and their mesentery in order to evaluate preferential seeding sites. Specific regions evaluated included peritoneal cavity lining, ovaries, lesser omentum, greater omentum (OFB), diaphragm, liver, stomach, pancreas, spleen, kidney, small intestine, small intestine mesentery, large intestine, and large intestine mesentery. Tumor size was scored as **(0)**: no visible tumor, **(1):** < 1mm; **(2):** 1–3mm; or **(3):** >3mm or solid mass. The maximum PCI score was 42, reflecting maximal lesion size in each of the 14 designated areas. Relative PCI scores were further validated by qRT-PCR analysis of FFL gene expression employed as a tumor cell reporter gene.

Tissue and peritoneal serous fluid harvest

The OFB was harvested from each mouse post-mortem, weighed, rinsed with $PBS^{-/-}$, and processed for FACS or placed into RNAlater (Qiagen) and stored at −80°C. Resident peritoneal cavity cells were collected via peritoneal lavage with 5ml of 1mM EDTA in $PBS^{-/-}$. The effluent was centrifuged, subjected to erythrocyte lysis (155mM NH_4Cl, 10mM $KHCO_3$, 0.1mM EDTA), and further processed as described below.

Tissue digest

SVFs were isolated by digesting individual OFBs (n=4–6) in GKN-buffer containing 1.8mg/ml Type IV collagenase, 10% FBS, and 0.1mg/ml DNase as previously described (10). Following digest at 37°C for 45 min, cells were passed through a 40μm cell strainer, and erythrocytes were lysed (see above).

FACS analysis

Single cell suspensions derived from OFB and PSF were washed in flow buffer (2% BSA in $PBS^{-/-}$), blocked with Fc block (BD Biosciences) for 10 minutes at 4°C, rinsed and incubated with fluorochrome-labeled antibody combinations (available upon request) for 20 min at 4°C. Antibodies specific for mouse CD45, CD11b, CD11c, F4/80, Ly6C, CD4, CD44, CD62L, B220, CD19, NK1.1, and Ly6G were obtained from eBioscience. CD3 and CD8 antibodies were obtained from BD Biosciences. Prior to analysis, cells were washed twice and resuspended in $PBS^{-/-}$ with propidium iodide for dead cell exclusion. FACS was

performed on a FACSAria (BD Biosciences) and data was analyzed using Flowjo (TreeStar) software.

Quantitative real-time PCR (qRT-PCR)

Individual OFBs were homogenized in Qiazol (Qiagen) and RNA was purified using an RNeasy Lipid Tissue Kit (Qiagen), according to manufacturer's instructions. RNA concentration was determined using a NanoDrop1000 spectrophotometer. RNA (n=4–6) was subjected to the iScript cDNA synthesis system (Biorad) according to manufacturer's protocol. qRT-PCR was performed with 12.5ng cDNA per sample using gene-specific SYBR Green primers (primer sequences are available upon request) designed with Beacon Design software. SensiMix SYBR and Fluorescein mastermix (Bioline) was used in a 15μL reaction volume. qRT-PCR was performed for 42 cycles at 95°C for 15 sec, 60°C for 15 sec, and 72°C for 15 sec, preceded by a 10 min incubation at 95°C on the iQ5 (Biorad). Melt curves were performed to ensure fidelity of the PCR product. The housekeeping gene was *L19* (10) and the ΔΔCt method (16) was used to determine fold differences.

Statistical analysis

Data are expressed as mean ± standard error of mean (SEM). FACS and qRT-PCR data were analyzed using a one-way ANOVA coupled with a Tukey Post-hoc test in SigmaPlot (Systat Software). Differences were considered statistically significant at $p<0.05$.

RESULTS

OFB size and cellularity

The size of the OFB increased significantly with age between five-month and eleven-month old nulliparous mice, coinciding with overall age-associated weight gain of the animals (14.4g ± 1.5 and 28.2g ± 2.2, $p<0.01$). Parity was associated with an additional increase in OFB weight (Figure 1A, $p<0.01$), although the average body weight of these age-matched groups were not significantly different (29.8g ± 0.8 vs 31.7g ± 0.7). The OFB SVF cell count was significantly elevated as a function of both age and parity, increasing 800% in parous mice (Figure 1B, $p<0.01$). Therefore, parity induced a change in stromal vascular cell influx or proliferation and not just an increase in overall OFB adiposity. The proportion of $CD45^+$ leukocytes represented approximately 50% of the SVF in both sets of nulliparous mice but >95% of the SVF in parous mice (Figure 1C, $p<0.01$). In order to further define the age- and parity-associated signature, we evaluated expression of a set of immune-related genes using qRT-PCR on whole tissue samples. As shown in Figure 1D, there were both age-and parity-associated differences in the expression of a number of important cytokines and chemokines in the homeostatic state. Notably, in mature nulliparous animals, the expression of chemotactic molecules for monocytes (*Ccl1*, *Ccl4* and *Ccl7*, $p<0.05$) as compared to young nulliparous mice was increased. Expression of *Tgfβ*, an important regulator of tumor cell invasion and metastasis, was significantly higher in older mice, irrespective of parity ($p<0.01$). Parity-specific changes included a significantly lower expression of neutrophil chemoattractants (*Cxcl1*, *Cxcl2*, $p<0.05$), and alternative activation-related genes characteristic of tumor-associated macrophages (*Arg1*, *M6pr*, $p<0.05$). Thus, inherent changes that occur as a result of aging and child-bearing can affect the signaling milieu in the OFB.

OFB SVF characterization

The OFB SVF was further characterized via FACS analysis to identify age- and parity-specific differences in immune cell composition. Viable cells (propidium iodide exclusion) were separated into $CD45^+$ leukocytes and $CD45^-$ stromal constituents. $CD45^+$ cells were

subsequently separated into R1 (lymphocyte) and R2 (monocyte/granulocyte) gates based on forward/side scatter (Figure 2A), and leukocyte subsets were identified based on well-defined surface markers. The $CD45^+$ subsets associated with the OFB in nulliparous mice were comparable, irrespective of age. However, the immune cell composition of the parous OFB was strikingly different, supporting the hypothesis that parity leads to establishment of a unique protective microenvironment. In the OFB of nulliparous mice the lymphocyte to monocyte/granulocyte (R1:R2) ratios were approximately 6:4 independent of age, whereas lymphocytes represented almost 90% of the leukocytes isolated from the parous OFB (Figure 2B). This was mirrored in the peritoneal serous fluid (PSF), denoted by a 20% increase in the proportion of lymphocytes to monocytes/granulocytes in parous mice as compared to mature nulliparous mice ($p<0.05$, Supplementary Table S1).

The parity-associated increase in lymphocytes was reflected across numerous subsets including $CD3^+$ T-cells ($p<0.01$), $CD19^+$ B-cells ($p<0.05$) and $CD11c^+$ dendritic cells (DCs) ($p<0.01$) with concomitant decreases in $F480^+$ macrophages ($p<0.01$) and $NK1.1^+$ NK-cells ($p<0.01$) compared to nulliparous mice (Figure 2C). Compared to their nulliparous counterparts, the parous OFB also displayed significantly increased $CD3^+CD4^+$ T_H-cells, and significantly decreased $CD3^+CD8^+$ T_C and $CD3+CD4^-CD8^-$ cells ($p<0.05$, Figure 2D). Parity also induced a significant increase in the proportion of T-cells and B-cells in the PSF, although levels of NK cells and DCs were unchanged ($p<0.05$, Supplementary Table S1).

Notably, there was a significant parity-associated shift in the subsets of B-cells residing in the OFB. $CD11b^+B220^{lo/+}$ B1-cells were the most prevalent subset of B-cells in nulliparous mice, whereas in parous mice the $CD11b^-$ $B220^{lo/+}$ B2-subset was dominant (Figure 2E). B1-cells are the predominant B-cell type in the peritoneal cavity, and are considered a more “innate-like” population, with receptors for autoantibodies and conserved bacterial and viral epitopes (17). This increase in B2-cells could be indicative of a more systemically active humoral B-cell response in parous mice.

Parity-associated changes were also evident within OFB macrophage subsets, although these changes were not mirrored in the parous PSF. In the PSF, macrophages are typically subdivided into “large peritoneal macrophages” (LPMs), and “small peritoneal macrophages” (SPMs) (18). LPMs can be distinguished via FACS based on forward/side scatter and higher CD11b and F480 surface staining. SPMs increase in the PSF as a result of LPS stimulation, and are derived from blood monocytes (18). The applicability of these subsets to the OFB is largely undefined. Here, the PSF contained mostly LPMs in the homeostatic state, with SPMs representing only a minor fraction of the total macrophage population. This trend was not significantly altered by parity (data not shown). In contrast, whereas the predominant macrophage population in the OFB of nulliparous mice was the $CD11b^+F480^{lo}$ population (SPMs), this population was significantly reduced in parous mice. Further, the $CD11b^+F480^+$ population (LPMs) was virtually undetectable in parous mice, although it represented approximately 8% of the R2 gate in nulliparous mice (Figure 2F). Collectively, this data suggest that nulliparous mice, irrespective of age, had similar immunomodulatory microenvironments in the peritoneal cavity as denoted by indistinguishable leukocyte profiles at these timepoints.

Impact of parity on peritoneal tumor burden

As parous women have a decreased risk of ovarian cancer, we next evaluated whether the parous microenvironment was more refractory to tumor cell seeding and outgrowth. To investigate this, we utilized a highly aggressive variant of our MOSE-L cells (MOSE-L_{FFLv}). Implantation of these cells results in rapid and widespread peritoneal outgrowth and ascites in syngeneic C57BL/6 female mice. At 21 days post-injection of 1×10^4 MOSE-L_{FFLv} cells, nulliparous and parous mice were euthanized and the peritoneal cancer index

(PCI) was assessed. Young nulliparous mice were chosen for comparison, since only minor changes in gene expression and no notable changes in the immune microenvironments were noted between young and mature nulliparous groups. We reasoned that these comparisons would provide additional insights into mechanistic alterations in the immune microenvironment as a consequence of peritoneal tumor dissemination. Notably, parous mice had a significantly decreased PCI compared to nulliparous mice (Figure 3A; $p<0.01$). To confirm this, we determined relative levels of the FFL reporter gene in the OFB using qRT-PCR. FFL expression, as evidenced by lower ΔCt values (normalized to the housekeeping gene L19), was signficantly higher in the OFB of MOSE-L_{FFLv}-injected nulliparous mice than in parous mice ($p<0.05$; Figure 3B). The OFB from $PBS^{-/-}$ injected mice were negative for FFL reporter gene expression.

Macroscopically, the OFBs in nulliparous mice were devoid of residual adipose tissue and were fully overtaken by fibrous tumor tissue. The average OFB weight increased significantly in cancer-bearing nulliparous mice (Figure 3C) and 60% of mice developed bloody ascites. In contrast, cancer-bearing parous mice presented with visible individual tumor nodules throughout the OFB, but residual adipose tissue was still highly evident, and no ascites was observed. The OFB weight did not change between MOSE-L_{FFLv}- and vehicle-injected parous mice, confirming a significantly lower OFB tumor burden than in nulliparous mice.

The aggressive growth of MOSE-L_{FFLv} cells in nulliparous animals coincided with a 15-fold increase in the SVF cell count of the OFB (Figure 3D), although the proportion of $CD45^+$ leukocytes did not change (Figure 3E). This suggests that the tumor microenvironment induced a proliferation or influx of leukocytes and $CD45^-$ stromal constituents. This trend was not observed in parous mice (Figure 3D,E), indicating that the OFB microenvironment of parous animals is inherently more resistant to either tumor outgrowth or the recruitment of pro-tumorigenic factors or cell types.

OFB SVF characterization with ovarian cancer

The OFB and PSF of ovarian cancer-bearing mice were further characterized via FACS analysis to determine the impact of cancer cell seeding on leukocyte populations. Tumor outgrowth caused a reduction in the proportion of lymphocytes and a concomitant increase in monocyte/granulocytes in the OFB, irrespective of parity (Figure 4A). This pattern was also evident in the PSF, with an increase in the proportion of monocytes/granulocytes of both nulliparous (19% ± 11.0, $p=0.21$) and parous mice (15% ± 1.6, $p<0.01$) (Supplementary Table S2).

Most notably, there was a significant increase in the $CD11b^+Ly6C^+$ $Ly6G^+$ population (Figure 4B; $p<0.001$) as a result of cancer cell seeding in the OFB. This population resembles the previously described $CD11b^+Ly6C^+Ly6G^+$ tumor-associated neutrophil population (TANs) (19). Additionally, the cancer-associated re-distribution of R1:R2 leukocytes in the OFB of nulliparous mice was mirrored across all subsets with decreased $CD3^+$ T-cells, $CD19^+$ B-cells, and $NK1.1^+$ NK-cells, and concomitant increases in $F480^+$ macrophages and $CD11c^+$ DCs. While levels of T_H-cells and T_C-cells declined with cancer seeding, both double negative ($CD3+CD4^-CD8^-$: DN-T cells) and NK-T cell subsets increased although significance was not quite reached (Figure 4C). The DN T-cells may represent either an immunosuppressive T-cell population that secretes *Tgfβ* and *Il-10* and directly kills cytotoxic T-cells (20) or γδ T-cells (20,21) albeit neither γδ TCR expression nor intracellular cytokine expression were examined in this study.

No differences in the proportions of B1- and B2-lymphocytes were noted in the OFB of cancer-bearing nulliparous animals (Figure 4D). However in the PSF, the B1:B2 ratio

increased from 3:1 in the homeostatic state to 5:1 due to MOSE-L_{FFLv} implantation ($p<0.05$, data not shown). As B1-cells act as the bridge between innate and adaptive immunity, producing low-affinity antibodies, this may be reflective of an ineffective humoral immune response similar to human patients that present with anti-tumor antibodies that afford no disease protection (22). It is important to note that while the proportion of B1:B2 cells increased with cancer, the overall percentage of both B1- and B2-cells in the PSF leukocyte population actually decreased as a result of shifting R1:R2 ratios. Further, the $CD11b^{lo/+}F480^{-}$ monocyte subset levels significantly decreased as a result of cancer (Figure 4E). Therefore, the cancer-associated OFB immune profile in nulliparous mice included increased proportions of TANs and macrophages and decreased lymphocyte and monocyte populations.

To complement our FACS analysis, we utilized qRT-PCR to characterize the overall signaling milieu of the OFB microenvironment after peritoneal cancer dissemination. Expression patterns represent the tissue as a whole, and thus are reflective of adipocytes, the SVF, and cancer cells within the tissue. A panel of cytokines and chemokines was used to provide an overview of genes that may contribute to a pro-tumorigenic microenvironment (Supplementary Table S3–4). The expression of B-cell chemoattractants (*Cxcl13*, *Il-5*) was significantly lower while monocyte-associated cytokines (*Ccl2*, *Ccl20*, *inos*, *Arg1*, *Ym1*) and neutrophil chemoattractants (*Cxcl1*, *Cxcl3*, *Cxcl5*, *Cccl3*) were significantly higher in nulliparous mice after cancer seeding (Figure 4F). These changes in the microenvironmental transcriptome support the cellular changes found in the SVF, namely the decrease in B-cells and approximately 100-fold increase in TANs in the OFB of cancer-bearing nulliparous mice.

In contrast to nulliparous animals, there was no significant net gain of leukocytes in the OFB of parous animals after tumor outgrowth (see Figure 3D,E). However, a similar cancer-associated shift in the leukocyte subsets was detected, denoted by a decline in T- and B-cells and an increase in macrophages and TANs (Figure 5A). Among $CD3^{+}$ leukocytes (Figure 5B), only an increase in the $CD4^{-}$, $CD8^{-}$ double negative subset was noted as a consequence of tumor outgrowth. The influx of the TANs was significantly reduced, representing only 7% of the $CD45^{+}$ population in parous mice, as opposed to the 25% in nulliparous animals (see also Figure 4B). This suggests that cancer-mediated recruitment of TANs to the OFB may be compromised or dampened as a consequence of parity. It should also be noted that all lymphocyte subsets were maintained at high levels in the OFB of parous animals, irrespective of cancer, which may help to maintain an activated state that is less conducive to cancer cell proliferation. This is further supported by the B-cell subset distribution shift towards the B2 phenotype in parous animals (Figure 5C), which contrasts that observed in nulliparous animals (Figure 4D). Unlike nulliparous mice, there was no significant cancer-associated decline in $CD11b^{lo/+}F480^{+}$ monocytes in parous mice (Figure 5D). However, these levels were already significantly elevated in the homeostatic parous OFB.

TANs in the parous PSF were elevated as a result of cancer ($p<0.01$, Supplementary Table S2), albeit at a lower level than in nulliparous mice. Additionally, the PSF in parous animals displayed a loss of LPMs and an increase in SPMs after MOSE-L_{FFLv} dissemination. The recruitment of SPMs is indicative of an innate-like inflammatory response, thus parous animals may be able to override, at least transiently, the inherent immunosuppressive program elicited by the MOSE-L_{FFLv} cells.

Comparative assessment of the gene expression profile of the parous OFB revealed that the expression of neutrophil chemoattractants was significantly higher in cancer-bearing mice (*Cxcl1*, *Cxcl2*, *Cxcl3*, *Cxcl5*; Figure 5E). This correlates with the recruitment of TANs

following cancer cell seeding, highlighting the importance of TANs in the propagation of the pro-tumorigenic microenvironment. Together, our data suggests that the pre-existing parity-associated microenvironment within the peritoneal cavity is inherently more resistant to tumor cell seeding and outgrowth by virtue of its ability to modulate recruitment of pro-tumorigenic immune cell types, either before tumor cell attachment (pre-metastatic niche) or following seeding and outgrowth.

DISCUSSION

Epidemiological studies indicate that parity reduces the risk of both ovarian and breast cancer development. While the molecular mechanisms of decreased ovarian cancer occurrence remain unclear, breast cancer studies suggest that protective effects relate to decreased cancer metastasis (3). It is possible that child-bearing results in a naturally occurring protective state that could be harnessed and utilized in the treatment of ovarian cancer, preventing fatal metastatic outgrowth. Our results demonstrate that parity, but not age, altered the OFB immune profile in the homeostatic state. This parity-associated immune profile was positively correlated with reduced peritoneal tumor burden. A more comprehensive understanding of the dynamic cellular interactions during metastatic outgrowth is critical for the development of treatment strategies to effectively target the tumor microenvironment at the time of disease discovery. These insights may ultimately lead to novel strategies to re-polarize the immune microenvironment of the OFB in a manner that reflects a microenvironment refractory to cancer growth.

Here, we compared the immune profile of the OFB as a function of age and parity to assess whether a pre-existing microenvironment exists that may be refractory to tumor growth. To this end, we characterized the leukocyte composition and cytokine expression profiles of the OFB and PSF, both in the homeostatic state and after aggressive ovarian cancer cell implantation. In the homeostatic state, parity (but not age) resulted in a marked decrease in monocytic cell subsets and affiliated chemoattractants, and a shift to predominantly B2-, as opposed to B1 B-lymphocytes. Following syngeneic cancer cell implantation, parous mice exhibited a significantly reduced tumor burden as compared to nulliparous mice. The tumor microenvironment was denoted by higher TANs and TAMs, and an increase in B1-cells in nulliparous animals, a trend that was dampened in parous mice in conjunction with decreased tumor growth. Thus, we postulate that the parous OFB compositional profile is indicative of a pre-existing niche that is partially refractory to metastasis.

In order to more fully elucidate an expression signature indicative of an inherently protective immune microenvironment in the parous state, we evaluated a panel of immunoregulatory cytokines and chemokines. Figure 6 summarizes all statistically significant gene expression changes associated with age, parity, cancer metastasis, or any combination therein ($p<0.05$; see Supplementary Table S3–4 for full list of genes evaluated). Age-related changes included a significantly increased expression of *Cxcl13* and *Il-2* in the OFB. *Cxcl13* is a B-cell chemoattractant and *Il-2* induces the proliferation and activation of T-cells; both are important signaling molecules in secondary lymphoid organs. Parity (but not age) was associated with a significant decrease in several chemoattractants for neutrophils (*Cxcl1*, *Cxcl2*; $p<0.05$) and monocytes (*Ccl2*, *Mcsf* $p<0.05$), as well as markers associated with alternately activated, pro-tumorigenic phenotypes (*Arg1*, *M6pr*, $p<0.05$). This correlates with the observed reduction of these cell types in the parous OFB, and may represent a metastasis-resistant microenvironmental signature. The most conspicuous cancer-related finding was the significant increase in neutrophil chemoattractants (*Ccl3*, *Cxcl1*, *-2*, *-3* and *-5*). Cancer-bearing groups also exhibited increased *Arg1* expression, and young adult nulliparous mice had increased *Ym1* expression, indicative of the presence of TAMs.

Given the pro-tumorigenic nature of TAMs (23,24), TANs (25,26), and myeloid-derived suppressor cells (27,28), the cancer-related increase in these cell types was expected. Therefore, the dampened influx of these subsets in parous mice may partially define the pre-existing protective niche in the OFB. In other words, parity leads to a reduction in the levels of cell subsets targeted for pro-tumorigenic polarization. A microenvironment that lacks these subsets, or is partially refractory to cancer-associated recruitment may slow the dynamics of tumor seeding and growth, resulting in delayed disease development.

The parous OFB also contained a greater proportion of both T- and B-lymphocytes. Tumor-infiltrating lymphocytes (TILs) correlate with improved prognosis and survival in a variety of murine and human cancer models (29–31). Therefore, a net gain in lymphocytes may be another attribute of the protective parity signature in the OFB. While the effects of increased T-cell populations in the tumor microenvironment have been well defined, less information is available describing tumor-infiltrating B-cells (TIL-Bs) and their impact on cancer progression (32). The presence of $CD20^+$ B-cells together with $CD8^+$ T-cells in the tumor microenvironment has been attributed to higher survival rates than the occurrence of either cell type alone, indicating a protective cellular signature (33). Interestingly, TIL-Bs produce granzyme B upon IL-21 stimulation, which would be cytotoxic to tumors; upon IFNα or TLR agonist stimulation, they can directly kill tumor cells via TRAIL signaling (34,35), also supportive of their anti-tumorigenic potential. In contrast, killer B-cells produce apoptotic death-inducing ligands including Fas ligand (FasL), TRAIL and programmed death ligands 1 and 2 (PD-L1, PD-L2) (36). However, their presence in the tumor microenvironment actually inhibits protective immune responses, inducing apoptosis of cytolytic effector cells instead of malignant cells (36). Regulatory B-cells, characterized by TGFβ and IL-10, also dampen and inhibit protective immune responses against tumors (37) by impairing T-cell priming. Hence, B-lymphocyte subsets are gaining widespread acceptance as key regulators and modulators of both pro- and anti-tumorigenic responses.

In this study, there was a shift in the B cell distribution of B1- and B2-cells as a consequence of parity, with B2-cells increasing significantly in the parous OFB. B1-cells play an important role in immunosurveillance in the peritoneal cavity, and are in a constant flux between the PSF and the OFB. During infection, B1-cells generate large amounts of low-affinity IgM, IgA and IgG3, ensuring early protection (38). B1-cells have been described as the precursors of tumor-promoting regulatory B-cells (B-regs) (39). B1-cells also possess many of the abovementioned regulatory properties, including constitutive FasL and PD-L 2 expression and the ability to produce IL-10. While the B2 subset is predominant in the parous OFB in the homeostatic state, with cancer cell seeding, the proportion of B1:B2 cells increases slightly in both parous and nulliparous mice. Collectively, this information may support the theory that B1-cells are subject to repolarization towards B-regs in the presence of cancer. Alternatively, the parity associated omental B2-cells may represent a subset such as the aforementioned killer B-cells that exhibit anti-tumorigenic activity. Future studies defining which B-cell subsets in parous animals are actually anti-tumorigenic will help clarify this question.

Parity was indeed associated with a significant reduction in tumor burden following syngeneic ovarian cancer cell implantation in the peritoneal cavity. The most significant cancer-associated finding was the increase in the proportion of TANs in the OFB. Hence, the ability to modulate early TAN infiltration may represent another protective element of the parous OFB. TANs are a significant portion of the inflammatory infiltrate in a variety of tumor microenvironments and numerous cancer cell lines express neutrophil chemoattractants, highlighting their importance in supporting the tumor milieu (40–43). Whereas depletion of TANs limits tumor metastasis, neutrophil accumulation in tumors is correlated with poor prognosis in clinical settings (41,44,45). The presence of TGFβ in the

tumor microenvironment is the driving factor in the polarization of neutrophils to a pro-tumorigenic (or "N2") type[46]. We found that *Tgfβ* expression was increased 100-fold in the OFB in both older nulliparous and parous animals. This age-related increase may play a crucial role in the increased ovarian cancer incidence in post-menopausal women. The decreased tumor burden observed in parous mice may be a result of decreased pro-tumorigenic subsets and chemoattractant expression (e.g. TANs and *Cxcl1, -2*) immediately available within the OFB, despite increased *Tgfβ* expression.

Parity also resulted in an almost complete loss of $CD45^-$ progenitor populations present within the OFB. An important component in the tumor cellular milieu is the stromal contingent. These cells are recruited from adipose tissue and bone marrow in order to provide crucial growth factors, matrices, cytokines and nutrients in order to support rapid tumor growth (47,48). The loss of progenitor cells in the OFB may reflect another aspect of the "protective signature" associated with child-bearing, in that the scaffolding or accessory cells crucial to rapid tumor growth are not initially available in situ. This may indicate a parity-associated differentiation or egress of $CD45^-$ progenitor populations within the OFB, in agreement with an increase in differentiation signals previously reported as part of a "parity signature" in mammary tissue (3).

The OFB is not only important as a preferential site for ovarian cancer, but also because of its role in peritoneal immunosurveillance. Its removal results in subsequent impaired antibacterial responses in the abdomen, and an increased chance of sepsis following surgery (5). Clearly, removal of this vital organ is not ideal, but it is generally regarded as necessary to help minimize recurrent disease. Our study suggests that a more comprehensive analysis of the parity-induced molecular and cellular changes within this immunologically- and metastatically-relevant microenvironment is needed in humans. Confirmation of a protective "parity-associated signature" in humans could help in the design of novel immunotherapies that induce or establish this inherent protective state (3).

In conclusion, our data supports epidemiological findings suggesting that child-bearing provides inherent partial protection against ovarian cancer (11,49,50). It is worth noting that the parity-associated protective microenvironment in the peritoneal cavity is only transient and eventually the outgrowth of cancer cells shifts the balance back towards a pro-tumorigenic state. Understanding what defines the transient nature of this refractory state may provide novel insights to modulate the OFB and prevent recurrent disease. While our studies do not address whether parity mitigates early stages of ovarian tumorigenesis, they do highlight a protective effect against peritoneal seeding and outgrowth. Future studies are clearly warranted to understand how the OFB could be re-polarized towards a parity-associated protective state in high-risk patients, or modulated to help delay or prevent recurrent disease in advanced stage ovarian cancer patients.

Supplementary Material

Refer to Web version on PubMed Central for supplementary material.

Acknowledgments

Special thanks to Melissa Makris for help with FACS experimental design and analysis. This manuscript fulfills in part the PhD dissertation requirements for C.A. Cohen in the Department of Biomedical Sciences and Pathobiology at Virginia Tech. C. A. Cohen was supported in part by a graduate research assistant fellowship provided by the VMRCVM at Virginia Tech.

Financial Support: This research was supported in part by NCI research grant CA118846 (E. Schmelz, P. Roberts) and funds provided by the Fralin Life Sciences Institute at Virginia Tech (P. Roberts, E. Schmelz).

References

1. Siegel R, Naishadham D, Jemal A. Cancer statistics, 2012. CA: A Cancer Journal for Clinicians. 2012; 62:10–29. [PubMed: 22237781]
2. Saad AF, Hu W, Sood AK. Microenvironment and pathogenesis of epithelial ovarian cancer. Hormones & Cancer. 2010; 1:277–290. [PubMed: 21761359]
3. Blakely CM, Stoddard AJ, Belka GK, Dugan KD, Notarfrancesco KL, Moody SE, et al. Hormone-induced protection against mammary tumorigenesis is conserved in multiple rat strains and identifies a core gene expression signature induced by pregnancy. Cancer Res. 2006; 66:6421–6431. [PubMed: 16778221]
4. Kenny HA, Dogan S, Zillhardt M, Mitra KA, Yamada SD, Krausz T, et al. Organotypic models of metastasis: A three-dimensional culture mimicking the human peritoneum and omentum for the study of the early steps of ovarian cancer metastasis. Cancer Treatment and Research. 2009; 149:335–351. [PubMed: 19763444]
5. Van Vugt E, Van Rijthoven EA, Kamperdijk EW, Beelen RH. Omental milky spots in the local immune response in the peritoneal cavity of rats. The Anatomical Record. 1996; 244:235–245. [PubMed: 8808398]
6. Gerber SA, Rybalko VY, Bigelow CE, Lugade AA, Foster TH, Frelinger JG, et al. Preferential attachment of peritoneal tumor metastases to omental immune aggregates and possible role of a unique vascular microenvironment in metastatic survival and growth. Am J Pathol. 2006; 169:1739–1752. [PubMed: 17071597]
7. Park HT, Lee ES, Cheon YP, Lee DR, Yang KS, Kim YT, Hur JY, et al. The relationship between fat depot-specific preadipocyte differentiation and metabolic syndrome in obese women. Clinical Endocrinol. 2012; 76:59–66.
8. Sorensen EW, Gerber SA, Sedlacek AL, Rybalko VY, Chan WM, Lord EM. Omental immune aggregates and tumor metastasis within the peritoneal cavity. Immunologic research. 2009; 45:185–194. [PubMed: 19253004]
9. Krishnan V, Stadick N, Clark R, Bainer R, Veneris JT, Khan S, et al. Using MKK4's metastasis suppressor function to identify and dissect cancer cell-microenvironment interactions during metastatic colonization. Cancer Metastasis Rev. 2012; 31:605–613. [PubMed: 22706843]
10. Cohen CA, Shea AA, Heffron CL, Schmelz EM, Roberts PC. Intra-Abdominal Fat Depots Represent Distinct Immunomodulatory Microenvironments: A Murine Model. PlosOne. 2013; 8:e66477.
11. Modugno F, Ness RB, Allen GO, Schildkraut JM, Davis FG, Goodman MT. Oral contraceptive use, reproductive history, and risk of epithelial ovarian cancer in women with and without endometriosis. Am J Obs Gyn. 2004; 191:733–740.
12. Roberts PC, Mottillo EP, Baxa AC, Heng HH, Doyon-Reale N, Gregoire L, et al. Sequential molecular and cellular events during neoplastic progression: a mouse syngeneic ovarian cancer model. Neoplasia. 2005; 7:944–956. [PubMed: 16242077]
13. Swainson L, Mongellaz C, Adjali O, Vicente R, Taylor N. Lentiviral transduction of immune cells. Methods Mol Biol. 2008; 415:301–320. [PubMed: 18370162]
14. Carmignani CP, Sugarbaker PH. Synchronous extraperitoneal and intraperitoneal dissemination of appendix cancer. Eur J Surgical Oncol. 2004; 30:864–868.
15. Otto J, Jansen PL, Lucas S, Schumpelick V, Jansen M. Reduction of peritoneal carcinomatosis by intraperitoneal administration of phospholipids in rats. BMC Cancer. 2007; 7:104. [PubMed: 17584925]
16. Schmittgen TD, Livak KJ. Analyzing real-time PCR data by the comparative C(T) method. Nature Protocols. 2008; 3:1101–1108.
17. Montecino-Rodriguez E, Dorshkind K. New perspectives in B-1 B cell development and function. Trends Immunol. 2006; 27:428–433. [PubMed: 16861037]
18. Ghosn EE, Cassado AA, Govoni GR, Fukuhara T, Yang Y, Monack DM, et al. Two physically, functionally, and developmentally distinct peritoneal macrophage subsets. Proc Natl Acad Sci U S A. 2010; 107:2568–2573. [PubMed: 20133793]

19. Fridlender ZG, Sun J, Mishalian I, Singhal S, Cheng G, Kapoor V, et al. Transcriptomic analysis comparing tumor-associated neutrophils with granulocytic myeloid-derived suppressor cells and normal neutrophils. PLoS One. 2012; 7:e31524. [PubMed: 22348096]
20. D'Acquisto F, Crompton T. CD3+CD4−CD8− (double negative) T cells: saviours or villains of the immune response? Biochem Pharmacol. 2011; 82:333–340. [PubMed: 21640713]
21. Lu Y, Wang X, Yan W, Wang H, Wang M, Wu D, et al. Liver TCRgammadelta(+) CD3(+) CD4(−) CD8(−) T cells contribute to murine hepatitis virus strain 3-induced hepatic injury through a TNF-alpha-dependent pathway. Mol Immunol. 2012; 52:229–236. [PubMed: 22750070]
22. Gumu E, Erdamar S, Demirel G, Horasanli K, Kendirci M, Miroglu C. Association of positive serum anti-p53 antibodies with poor prognosis in bladder cancer patients. Int J Urol. 2004; 11:1070–1077. [PubMed: 15663677]
23. Sica A, Schioppa T, Mantovani A, Allavena P. Tumour-associated macrophages are a distinct M2 polarised population promoting tumour progression: potential targets of anti-cancer therapy. Eur J Cancer. 2006; 42:717–727. [PubMed: 16520032]
24. Mantovani A, Schioppa T, Porta C, Allavena P, Sica A. Role of tumor-associated macrophages in tumor progression and invasion. Cancer Metast Rev. 2006; 25:315–322.
25. Nozawa H, Chiu C, Hanahan D. Infiltrating neutrophils mediate the initial angiogenic switch in a mouse model of multistage carcinogenesis. Proc Natl Acad Sci U S A. 2006; 103:12493–12498. [PubMed: 16891410]
26. Piccard H, Muschel RJ, Opdenakker G. On the dual roles and polarized phenotypes of neutrophils in tumor development and progression. Crit Rev Oncology-Hem. 2012; 82:296–309.
27. Peranzoni E, Zilio S, Marigo I, Dolcetti L, Zanovello P, Mandruzzato S, et al. Myeloid-derived suppressor cell heterogeneity and subset definition. Curr Opin Immunol. 2010; 22:238–244. [PubMed: 20171075]
28. Dolcetti L, Peranzoni E, Ugel S, Marigo I, Fernandez Gomez A, Mesa C, et al. Hierarchy of immunosuppressive strength among myeloid-derived suppressor cell subsets is determined by GM-CSF. Eur J Immunol. 2010; 40:22–35. [PubMed: 19941314]
29. Pages F, Galon J, Dieu-Nosjean MC, Tartour E, Sautes-Fridman C, Fridman WH. Immune infiltration in human tumors: a prognostic factor that should not be ignored. Oncogene. 2010; 29:1093–1102. [PubMed: 19946335]
30. Dunn GP, Bruce AT, Ikeda H, Old LJ, Schreiber RD. Cancer immunoediting: from immunosurveillance to tumor escape. Nat Immunol. 2001; 3:991–998. [PubMed: 12407406]
31. Zhang L, Conejo-Garcia JR, Katsaros D, Gimotty PA, Massobrio M, Regnani G, et al. Intratumoral T cells, recurrence, and survival in epithelial ovarian cancer. New Eng J Med. 2003; 348:203–213. [PubMed: 12529460]
32. Spaner, D.; Bahlo, AB. Lymphocytes in Cancer Immunology. In: Medin, J.; Fowler, D., editors. Experimental and Applied Immunotherapy. Springer Science+Business Media; 2011. p. 37-55.
33. Milne K, Kobel M, Kalloger SE, Barnes RO, Gao D, Gilks CB, et al. Systematic analysis of immune infiltrates in high-grade serous ovarian cancer reveals CD20, FoxP3 and TIA-1 as positive prognostic factors. PLoS One. 2009; 4:e6412. [PubMed: 19641607]
34. Kemp TJ, Moore JM, Griffith TS. Human B cells express functional TRAIL/Apo-2 ligand after CpG-containing oligodeoxynucleotide stimulation. J Immunol. 2004; 173:892–899. [PubMed: 15240676]
35. Hagn M, Schwesinger E, Ebel V, Sontheimer K, Maier J, Beyer T, et al. Human B cells secrete granzyme B when recognizing viral antigens in the context of the acute phase cytokine IL-21. J Immunol. 2009; 183:1838–1845. [PubMed: 19592644]
36. Lundy SK, Killer B. lymphocytes: the evidence and the potential. Inflamm Research. 2009; 58:345–357.
37. Inoue S, Leitner WW, Golding B, Scott D. Inhibitory effects of B cells on antitumor immunity. Cancer Res. 2006; 66:7741–7747. [PubMed: 16885377]
38. Hansell CA, Nibbs RJ. The odd couple: innate-like B cells and the chemokine scavenger D6. Cell Cycle. 2011; 10:3619–3620. [PubMed: 22033177]
39. Lund FE. Cytokine-producing B lymphocytes-key regulators of immunity. Curr Opin Immunol. 2008; 20:332–338. [PubMed: 18417336]

40. Eck M, Schmausser B, Scheller K, Brandlein S, Muller-Hermelink HK. Pleiotropic effects of CXC chemokines in gastric carcinoma: differences in CXCL8 and CXCL1 expression between diffuse and intestinal types of gastric carcinoma. Clin Exp Immunol. 2003; 134:508–515. [PubMed: 14632759]
41. Jensen HK, Donskov F, Marcussen N, Nordsmark M, Lundbeck F, von der Maase H. Presence of intratumoral neutrophils is an independent prognostic factor in localized renal cell carcinoma. J Clin Oncol. 2009; 27:4709–4717. [PubMed: 19720929]
42. Wislez M, Rabbe N, Marchal J, Milleron B, Crestani B, Mayaud C, et al. Hepatocyte growth factor production by neutrophils infiltrating bronchioloalveolar subtype pulmonary adenocarcinoma: role in tumor progression and death. Cancer Res. 2003; 63:1405–1412. [PubMed: 12649206]
43. Ji H, Houghton AM, Mariani TJ, Perera S, Kim CB, Padera R, et al. K-ras activation generates an inflammatory response in lung tumors. Oncogene. 2006; 25:2105–2112. [PubMed: 16288213]
44. Pekarek LA, Starr BA, Toledano AY, Schreiber H. Inhibition of tumor growth by elimination of granulocytes. J Exp Med. 1995; 181:435–440. [PubMed: 7807024]
45. Tazawa H, Okada F, Kobayashi T, Tada M, Mori Y, Une Y, et al. Infiltration of neutrophils is required for acquisition of metastatic phenotype of benign murine fibrosarcoma cells: implication of inflammation-associated carcinogenesis and tumor progression. Am J Pathol. 2003; 163:2221–2232. [PubMed: 14633597]
46. Fridlender ZG, Sun J, Kim S, Kapoor V, Cheng G, Ling L, et al. Polarization of tumor-associated neutrophil phenotype by TGF-beta: “N1” versus “N2” TAN. Cancer Cell. 2009; 16:183–194. [PubMed: 19732719]
47. Ishii G, Sangai T, Oda T, Aoyagi Y, Hasebe T, Kanomata N, et al. Bone-marrow-derived myofibroblasts contribute to the cancer-induced stromal reaction. Biochem Biophys Res Commun. 2003; 309:232–240. [PubMed: 12943687]
48. Kidd S, Spaeth E, Watson K, Burks J, Lu H, Klopp A, et al. Origins of the tumor microenvironment: quantitative assessment of adipose-derived and bone marrow-derived stroma. PLoS One. 2012; 7:e30563. [PubMed: 22363446]
49. Merritt MA, De Pari M, Vitonis AF, Titus LJ, Cramer DW, Terry KL. Reproductive characteristics in relation to ovarian cancer risk by histologic pathways. Human reproduction. 2013; 28:1406–1417. [PubMed: 23315066]
50. Poole EM, Merritt MA, Jordan SJ, Yang HP, Hankinson SE, Park Y, et al. Hormonal and Reproductive Risk Factors for Epithelial Ovarian Cancer by Tumor Aggressiveness. Cancer Epidemiol Biomarkers Prev. 2013; 22:429–437. [PubMed: 23307531]

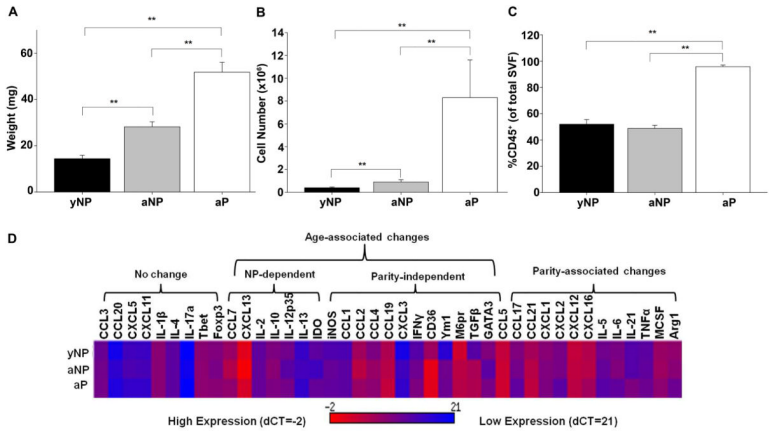

Figure 1.

Parity-associated differences in the cellularity of the OFBs of young adult nulliparous (yNP), mature adult nulliparous (aNP) and adult parous mice (aP) mice. **A)** Whole tissue OFB weight. **B)** Number of cells in the SVF isolated from digested OFB. **C)** $CD45^+$ population in OFB SVF. **D)** Gene expression profile of OFB. *p<0.05. **p<0.01.

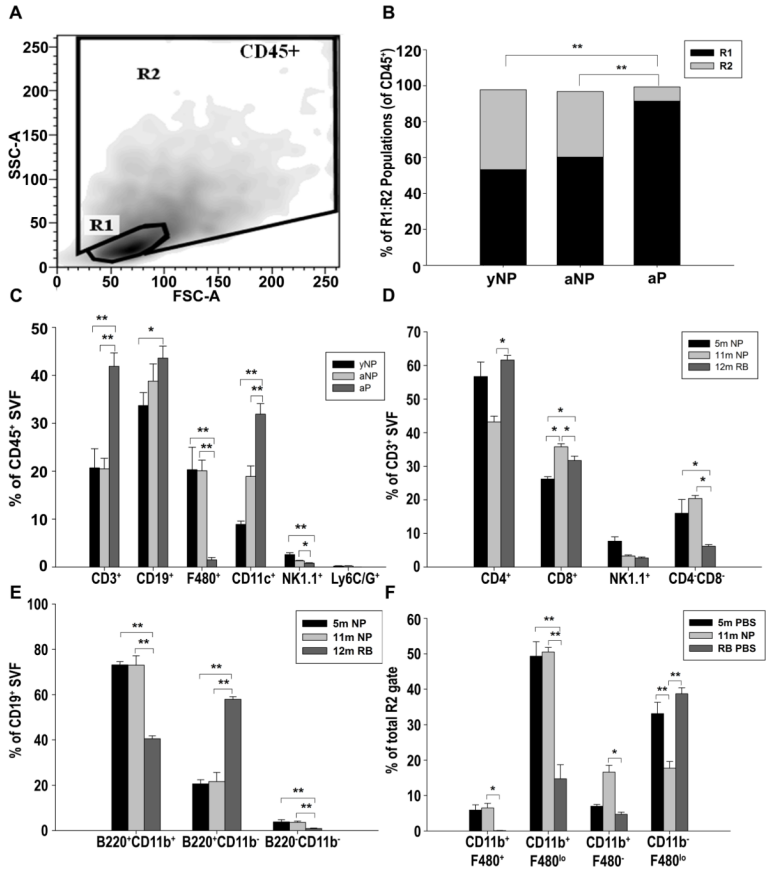

Figure 2.

The OFB displays parity-associated differences in leukocyte populations. **A)** $CD45^+$ leukocytes in the SVF of OFBs harvested from young adult nulliparous (yNP), mature adult nulliparous (aNP) and mature parous mice (aP) were separated into regions R1 (lymphocytes) and R2 (monocytes/granulocytes) for further analysis. **B)** Distribution of R1:R2 populations in OFBs. **C)** Overall immune cell populations in OFBs. **D)** $CD3^+$ subsets within OFBs. **E)** $CD19^+$ subsets within OFBs. **F)** Monocyte/granulocyte subsets within OFBs. *$p<0.05$, **$p<0.01$

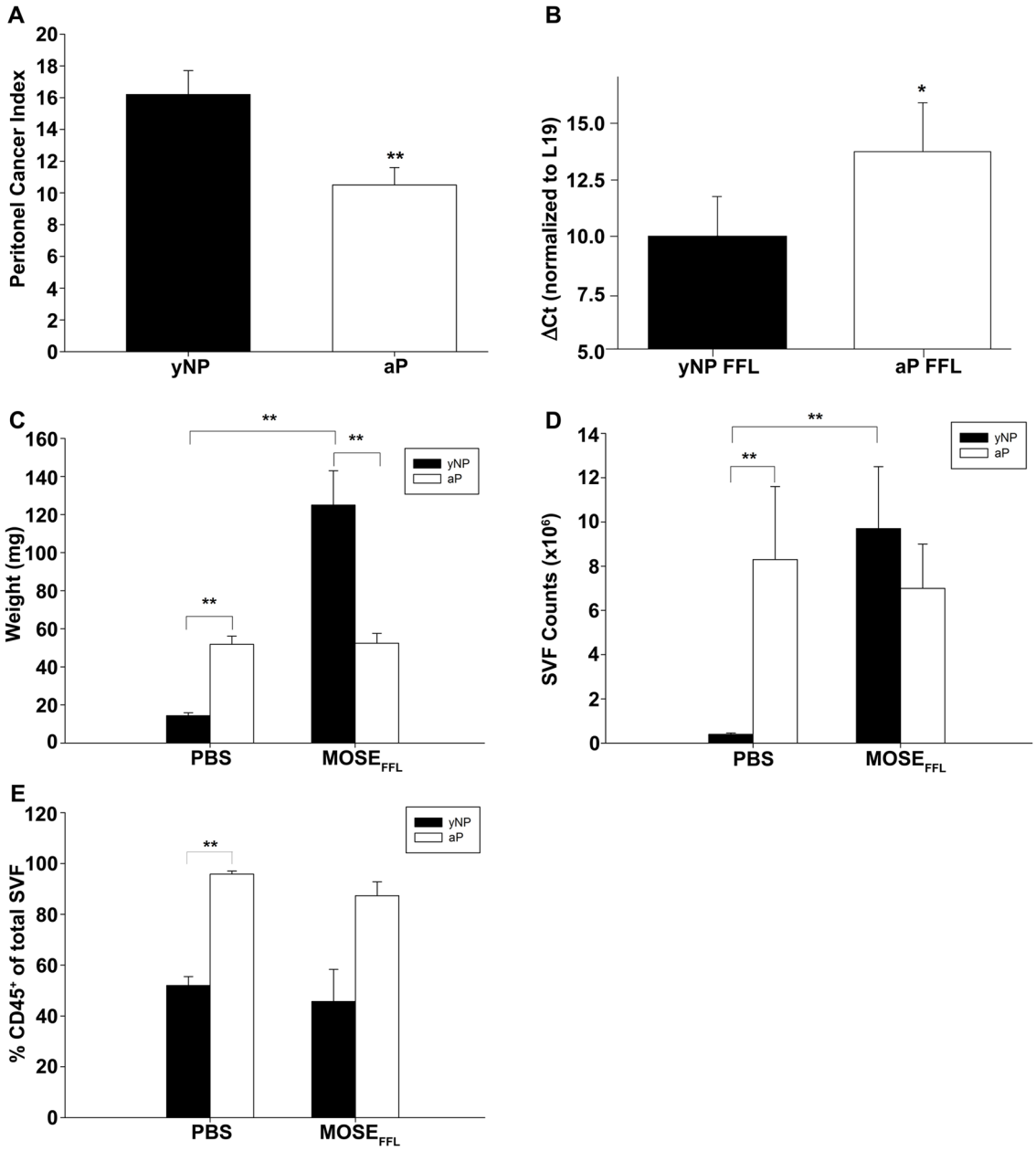

Figure 3.

Parity mitigates tumor burden and metastasis-associated influx of stromal cells to the OFB following $MOSE_{FFL}$ intraperitoneal implantation. Direct comparison of the SVF of OFBs obtained from young adult nulliparous (yNP) and mature adult parous (aP) mice without (PBS) or following MOSE-L_{FFLv} implantation. A) Peritoneal Cancer Index (PCI) (n =10). B) FFL gene expression in OFB of tumor-bearing mice compared to their PBS-injected counterparts. **C)** Whole tissue OFB weight. **D)** Total yield of SVF cells isolated from digested OFBs. **E)** Percentage of $CD45^+$ population in the OFB SVF. *p<0.05. **p<0.01.

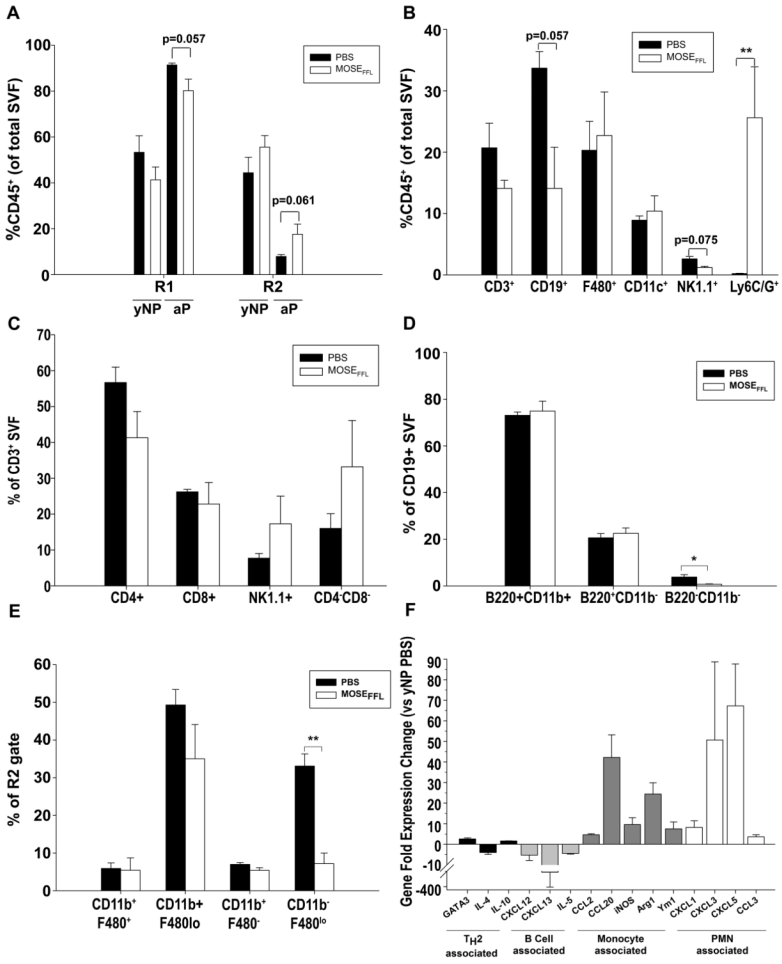

Figure 4.

Ovarian cancer outgrowth elicits macrophage and neutrophil influx into the OFB of young adult nulliparous (yNP) mice. **A)** Comparative distribution of R1(lymphocytes):R2(monocyte/granulocyte) CD45+ populations in yNP and mature adult parous (aP) OFB as a consequence of cancer dissemination. **B–D)** Immune cell changes in the OFB of yNP mice following MOSE-L_{FFLv} seeding and outgrowth were determined by FACS analysis. Overall leukocyte profile **(B)** and changes within $CD3^+$ subsets **(C)** $CD19^+$ subsets **(D)** and monocyte/granulocyte subsets **(E)** are depicted. **F)** Gene expression changes in the OFBs of MOSE-L_{FFLv}-bearing yNP mice compared to age-matched naïve mice (yNP PBS). All genes displayed were significantly ($p<0.05$) changed from PBS control. Statistical significance (p-values) are provided or denoted by * $p<0.05$. ** $p<0.01$.

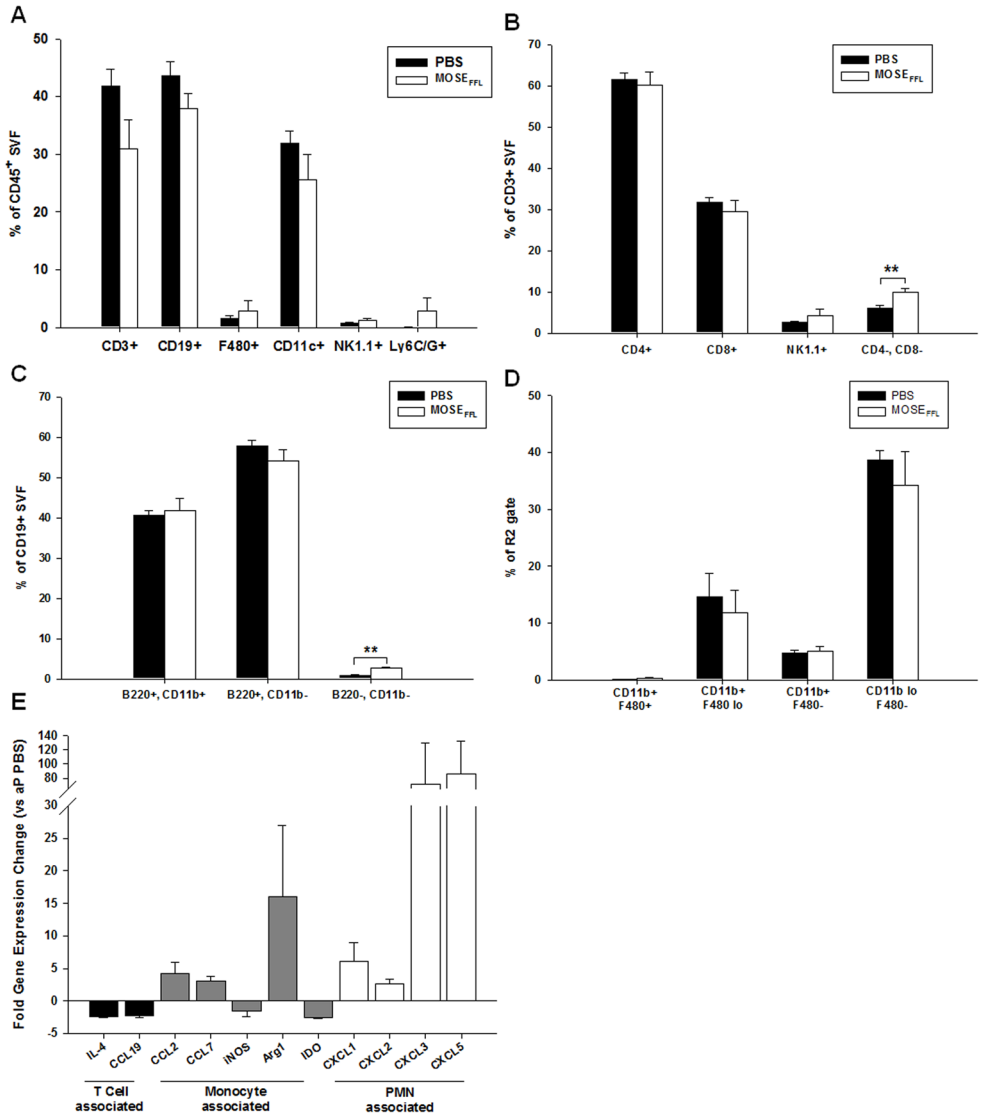

Figure 5.

Parity mitigates ovarian cancer outgrowth-associated influx of macrophages and neutrophils to the OFB. Immune cell changes in the OFB of mature adult (aP) mice following MOSE-L_{FFLv} seeding and outgrowth were determined by FACS analysis. Overall leukocyte population changes in the OFB **(A)** as well as cancer-associated changes within $CD3^+$ subsets **(B)**, $CD19^+$ subsets **(C)** and monocyte/granulocyte subsets **(D)** are presented. **F)** Gene expression changes in the OFBs of MOSE-L_{FFLv}-bearing aP mice compared to age-matched naïve mice (aP PBS). All genes displayed were significantly changed from PBS controls, *p<0.05. **p<0.01.

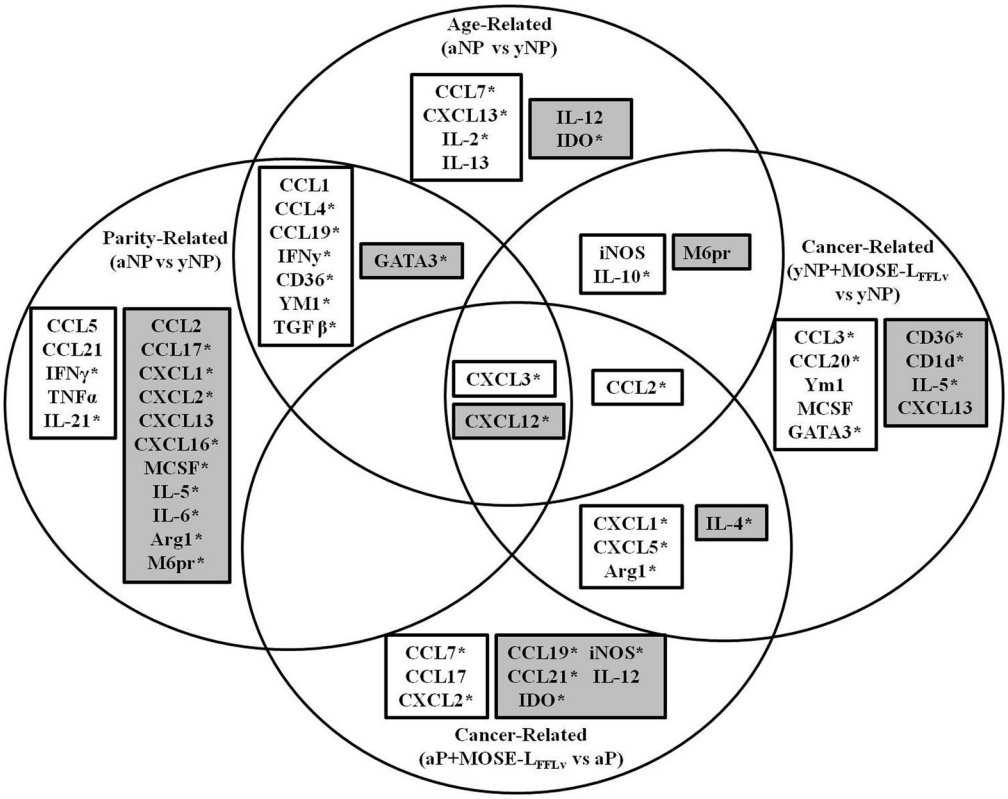

Figure 6.

Gene expression signatures in the OFB associated with age, parity, or cancer cell seeding and outgrowth. Venn diagram representing significantly altered genes (*), $p<0.05$, and genes trending towards significance $p=0.05–0.08$. White boxes indicate increased expression, grey boxes indicates decreased expression.